JOURNAL OF MATERIALS SCIENCE **38** (2003) 4003–4011

# A model material approach to the study of fracture process zone of quasi-brittle materials

E. JIMENEZ PIQUE*,‡
*Laboratory of Solid State Chemistry and Materials Science, Eindhoven University of Technology, P.O. Box 513, 5600MB Eindhoven, The Netherlands*
*E-mail: emilio.jimenez@upc.es*

L. DORTMANS
*TNO Institute of Applied Physics, P.O. Box 595, 5600 AN Eindhoven, The Netherlands*

G. DE WITH
*Laboratory of Solid State Chemistry and Materials Science, Eindhoven University of Technology, P.O. Box 513, 5600MB Eindhoven, The Netherlands*

A new approach to study the fracture of quasi-brittle materials is introduced: the design and testing of model materials. By model material is understood a material with enlarged microstructure and which material parameters, such as stacking and mechanical properties of particles and cohesion force, can be fully controlled. In this paper a first example to the model materials approach is presented, consisting in 5 mm steel particles bonded in a precise stacking with an epoxy-based glue. It is shown how it is possible to correlate the different fracture mechanisms and ultimate peak load of the model material to the particle pair force and to the fracture process zone size. It is also seen how a quasi-brittle behaviour is produced in the presence of mechanisms that induced the crack to shift fracture planes, that is, in presence of energy dissipative mechanisms. 

## 1. Introduction

Quasi-brittle fracture is, nowadays, one of the hottest topics in fracture mechanics because it is still not fully understood the relationship between the energy dissipative mechanisms in the fracture process zone and the macroscopical mechanical behaviour of the quasi-brittle materials. This type of quasi-brittle fracture can be found in several types of ceramics like toughened alumina, partially stabilized zirconia, refractory ceramics, cermets and composites, as well in several other materials like ice, polymers [1], rock [2] and some metals under certain conditions.

This behaviour is due to the existence of a number of different types of toughening mechanisms that shield the growth of the crack inside the fracture zone. Among these shielding mechanisms we find crack bridging, crack pinning, crack deflection (usually due to the addition of a second phase, zone shielding caused by residual thermal stresses), microcracking, phase transformation and shielding due to whiskers or fibres. All these different mechanisms interact in different ways with the crack growth and contribute to the loss of stiffness in the material. It has been suggested [3] that microcracking and, especially, bridging are the most important mechanisms present in this type of fracture. Not only all these effects contribute to the energy dissipation in front of the crack tip, but also they interact with each other, adding complexity to the problem.

The description of the fracture of these materials is quite complex, not only because all these shielding mechanism have to be taken into account, but also because the typical size of the specimen makes it impossible to apply the classical fracture mechanic tools. If the size of the process-zone is negligible compared to the size of the specimen the fracture behaviour can be described by linear elastic fracture mechanics, as it is the case of most brittle ceramics. If the size of the fracture process-zone covers almost all the sample, the failure is determined by a strength of yield stress criteria. However, if the fracture process zone has an intermediate size the fracture mechanism is much more complicated and can not be treated neither by linear elastic fracture mechanics (because the representative volume element has the same size as the fracture process zone) nor by strength criteria.

It is, therefore, necessary to identify the contribution of all the different shielding mechanisms, and to relate them to the macroscopic behaviour in order to establish an appropriate mathematical description of the fracture process zone and to better understand the inner behaviour of quasi-brittle ceramics during fracture.

*Author to whom all correspondence should be addressed.
‡*Present Address*: Dpto. Ciencia de los Materiales e Ingenería Metalúrgica, Universitat Politècnica de Catalunya, Avda. Diagonal 647 (ETSEIB), 08028 Barcelona (Spain).

There are several experimental techniques for inspecting and measure damage in quasi-brittle ceramics [4–12] (most of them coming from cement and concrete fields) as well as several models for roughly predicting the fracture behaviour [13–21], with enough precision for most engineering purposes. However, there are several fundamental questions to be answered related to the very (inner) nature of the material, i.e., to the physics of the fracture process zone of quasi-brittle ceramics, specially what is really happening inside the fracture process-zone and what are the most relevant parameters and their quantitative relationship with the macroscopic fracture behaviour. It is clear that, up to now, there is not much understanding of what is really happening inside the fracture process zone of quasi-brittle materials. It is then necessary to take a new approach to the problem.

## 2. The model material concept

Because there are a large number of parameters, all in the mesoscale range, the approach is simple: to enlarge the material itself by abstracting to a large model material with enlarged and controlled microstructural features. The scaling technique is widely used in engineering applications, and in some materials science problems [22], specially in plasticity and indentation problems [23].

By model material is understood as a material made up of large particles (choosing from micrometers to millimeters) in which its microstructural features can be controlled and manipulated reproducibly and independently within a sufficient large range. Controlling these microstructural features (bonding strength and behaviour, particle size and shape, existence of a second particle type, etc.) will alter in a different manner the overall macroscopical mechanical behaviour, including the fracture process zone size, giving then information about which microstructural parameters are the most relevant.

In other words, changing the scale of the microstructure and varying the relative contribution of the various dissipative mechanisms, which are controlled mainly by the type of bonding and size, type and shape of the particles, will change the macroscopical fracture behaviour. For example, if we use a tough spherical particle together with a brittle bond, this will result in a fracture path only in the bond area. On the other hand, if the particles have brittle behaviour, this will result in a transgranular fracture. If these same particles have an elongated shape but the same bonding force the fracture process will also be altered. All these changes will influence the macroscopical fracture behaviour and the length of the process zone.

It is really important to enlarge the size of the fracture process zone at the same time that the microstructure is enlarged. The size of the fracture process zone $\rho$ is [24]:

$$\rho = \frac{EG_f}{f_t^2} = \left(\frac{K_{Ic}}{f_t}\right)^2 \qquad (1)$$

where $E$ is the Young's modulus, $G_f$ the fracture energy, $K_{Ic}$ the fracture toughness, and $f_t$ the tensile strength.

Since the value of $E$ is approximately equal for the real and the model materials, the bonding between the particles has to be manipulated in such a way that the changes in the fracture energy, $G_f$, and the tensile strength, $f_t$, will result in a fracture process zone length enough to cover a significant number of grains.

The best choice is to use particles of hard material, and bind them together with a polymer. In this paper, a model material as simple as possible and large enough to manipulate with success the microstructure and orientation is presented, based, for convenience, on commercial available materials.

## 3. Experimental

The material particles or grains were simulated with 5 mm steel bearing balls (normally used for machine axes), and the cohesive force between grains were simulated with commercial available epoxy glues.

Once the 'particles' and the 'cohesive forces' were chosen, the material was implemented with a fixed size, number of particles and particle orientation: cubes of a thousand particles, with 5 cm in side (10 spheres) in a simple cubic stacking. Two orientations, with respect to the sample side, namely (100) and (110), were implemented, and two different epoxy glues were used to glue each sphere to the nearest neighbour.

The spheres were stainless steel bearing spheres (Steel Alloy 1020, annealed at 870°C) with a diameter of $5.000 \pm 0.001$ mm[1]. The Young's modulus of this steel is $E = 200$ GPa and yield strength is equal to 297 MPa, according to manufacturer specifications. The two glues were commercial available epoxy glues, cured by thermal treatment, and labelled as $A$[2] and $E$[3].

The Young's modulus of both Glue $A$ and Glue $E$ are comparable and equal to $2.4 \pm 0.2$ GPa, according to manufacturers specifications.

Materials produced with both orientations and glues were tested in a mode I fracture test. Moreover, single-edge notch beams tests on bulk glue to determine $K_{Ic}$, and two-particle fracture tests and wedge opening load tests for glue adhesion were performed.

### 3.1. Model materials implementation

The procedure to implement these materials is to force the spheres to the stacking and orientation we desire, by means of a physical constraint, in our case cylindrical pins, and glue them together by curing once the constraint has been removed.

In Fig. 1 a sketch of the entire procedure, for the (100) orientation, is shown. For (110) orientation the same procedure is followed, but rotating the pin array by 45°. First, the spheres were cleaned in successive ultrasonic baths of water, acetone and ethanol, 10 min each. Right after cleaning, the metal spheres were introduced into a cubic box with an array of removable vertical pins, with diameter equal to the interstitial diameter of a cubic array, that is, equal to $(1-\sqrt{2})*5 = 2.07$ mm. The

[1] provided by AKN Bearing Service.
[2] Araldite 2020, from Ciba Chemistry.
[3] Stycast 1654, from Emerson & Cuming Speciality Polymers.

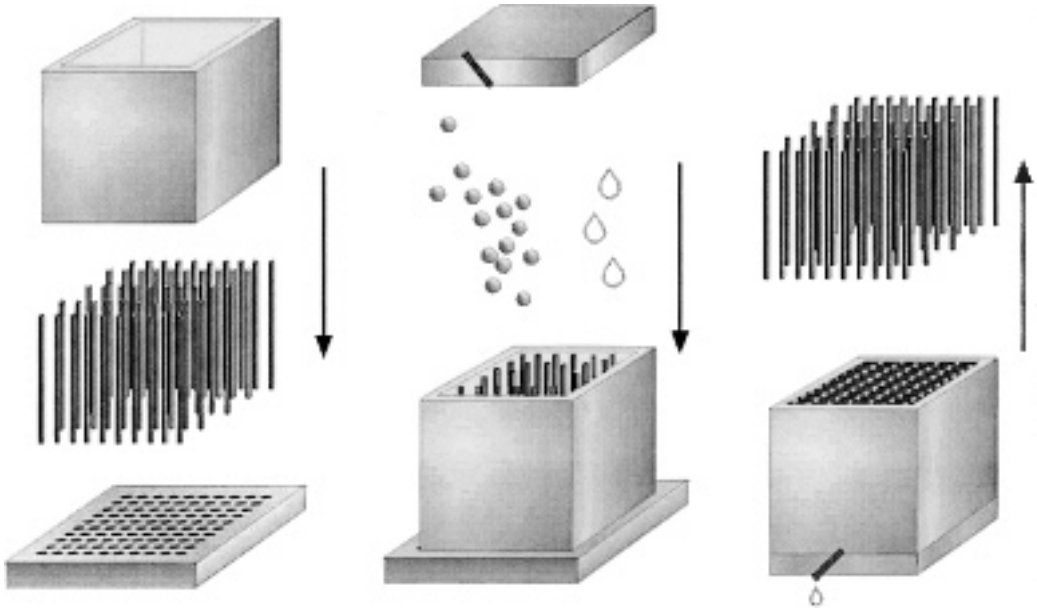

*Figure 1* The first step—left picture- is to set the pin array into the base and the box surrounding these pins. Once correctly placed, steel balls are poured—middle picture- in the box and forced by the pins to stack in a cubic stacking. Then the cube is filled with glue and the box is closed with a lid with a pipeline. Finally—right picture- the whole system is turn, the base and the pins are removed carefully and the cube is introduced in the furnace for glue curing.

role of these pins was to act as a constraint to the movement of the spheres, so they are forced to stack into a simple cubic staking and not the low energy close pack stacking. The walls of these cubes were made of steel covered on the inside with Teflon plates to avoid sticking to the walls. When all the spheres were placed in their position, the pins were removed carefully (so the spheres remained in their position) and glue was poured in the cube, allowing the excess of glue to drain out. This box was then introduced into a furnace for glue curing. The curing times and temperatures were 3 h at 60°C for glue *A* and 8 h at 45°C for glue *E*, both cured in air. After hardening of the glue and cooling, the model material was pulled out the box, being ready for testing. Fig. 2 present pictures of such model materials for both orientations, and Fig. 3 shows details of the interconnection between particles.

### 3.2. Bulk glue toughness

In order to determine the stress intensity factor, $K_{Ic}$, of the bulk glue, four point bending tests were performed on bulk glue single-edge notch beams (SENB). The dimensions of those bars were: length $l = 45$ mm, height $d = 4$ mm and width $w = 3$ mm. A first notch of 520 $\mu$m deep and 200 $\mu$m wide was machined in the middle of each sample. A second notch of 100 $\mu$m deep and 20 $\mu$m wide was machined using a diamond saw, exactly in the middle of the first notch, giving a total notch length, $a$, of 620 $\mu$m. The four point bending

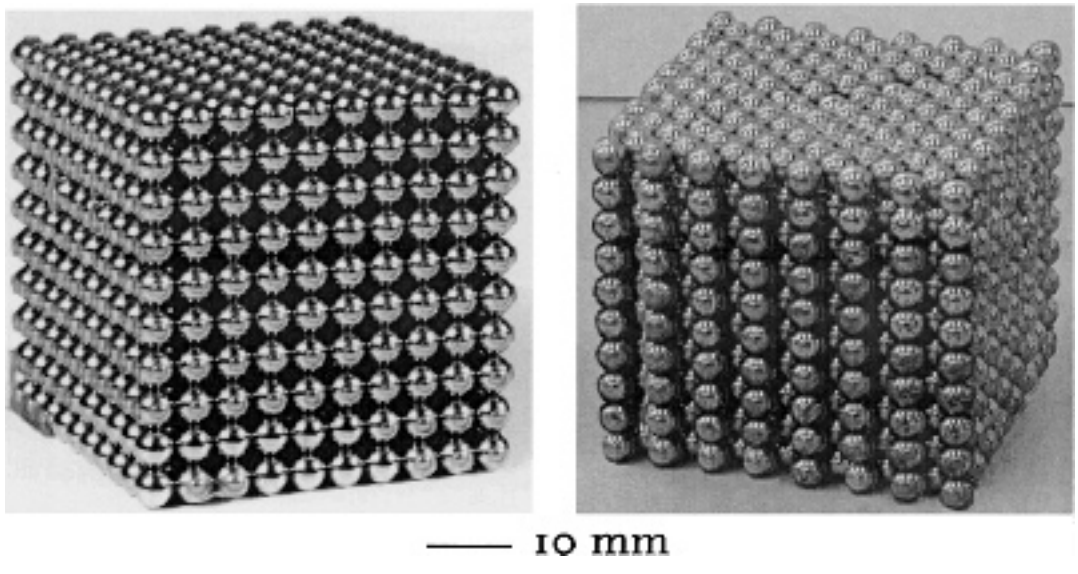


*Figure 2* Photograph of model material with (100) orientation—left- and (110) orientation—right-.

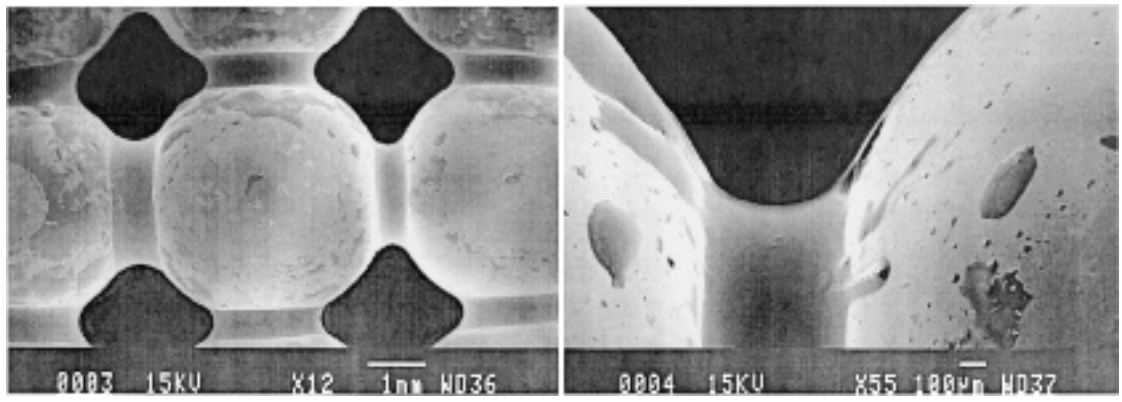


*Figure 3* Microphotographs of interconnection between particles of model material.

tests were performed in an Erichssen test machine at a speed of 5 mm/min. The separation of the rollers was 30 mm (lower rollers, $l_1$) and 5.60 mm (upper rollers, $l_2$).

The stress intensity factor, for this notch type, was calculated using the expression [25]:

$$K_{\mathrm{IC}} = F\frac{3(l_1 - l_2)}{2wd^2}\sqrt{a}\cdot Y(\alpha) \tag{2}$$

where $F$ is the fracture force and $Y(\alpha)$ is the geometry factor with $\alpha$ given by:

$$\alpha = \frac{a}{d} \tag{3}$$

Because this value $\alpha$ is lower than 0.6 and $\Delta l/d \approx 8$, we use the Gross-Srawely equation [26] to determine $Y(\alpha)$ as:

$$Y(\alpha) = 1.99 - 2.47\alpha + 12.97\alpha^2 - 23.17\alpha^3 + 24.8\alpha^4 \tag{4}$$

The stress intensity factor obtained for glue A was $K_{\mathrm{Ic}} = 0.85 \pm 0.05$ MPa $\mathrm{m}^{1/2}$ and for glue E was $K_{\mathrm{Ic}} = 1.11 \pm 0.02$ MPa $\mathrm{m}^{1/2}$.

### 3.3. Particle adhesion tests

The most important thing in characterizing the internal behaviour of our material is to know the mechanical behaviour of a particle pair. That is, how the 'grains' of the material are responding when the material is subjected to a mechanical test, in order to know which is the exact particle-particle force to match the microscopical behaviour to the overall fracture behaviour. These particles, because of the different orientation and the macroscopic loading used, will experience mode I fracture (in case of (100) orientation) or a mixed mode I/II fracture (in case of (110) orientation).

Therefore, in order to characterize the model material completely, tensile and shear fracture testing on single particle pairs were made. Particle pairs were produced with the same glues and curing times and temperatures as the model materials, and the tests were carried out in the Erichssen test machine at 5 mm/min. The results are shown in Table I.

### 3.4. Model material testing

Twelve cubes of model material were produced for testing. Six of them had (100) orientation and the other six had (110) orientation. For every orientation, three of the model materials were bonded with glue *A* and the other three with glue *E*. All the model materials produced (with both orientations) were tested in mode I performed in an Erichssen 476 test machine with a constant head speed of 5 mm/min, and force-displacement graphs were recorded.

For performing fracture test in the samples with (100) orientations, an initial notch of 10 mm along the middle of one of the faces was made during the construction of the model material. The reason for this notch was to have a measured initial crack from which the fracture started. The procedure was made as follows: when all the metal spheres are placed in the mould before the glue is poured, a teflon tape of 10 mm width and 100 $\mu$m thick and with a length of 50 mm is introduced in the middle of one of the faces perpendicular to the surface. This tape is then blocking the creation of a glue connexion between two rows of spheres. After pouring the glue and curing, the Teflon tape is removed. The glue connexions between spheres where the Teflon tape used to be, were then not formed, being an initial notch of 10 mm length. In this notch, a wedge with an opening angle of 45° connected to the head of the testing machine was inserted and the fracture tests were performed. In Fig. 6 a sketch of the wedge and the model material is shown. The splitting force ($F$) is then related with the applied force ($P$), if friction is neglected, via:

$$F = \frac{P}{2\tan(\beta/2)} \tag{5}$$

where $\beta$ is the angle of the wedge.

In Fig. 4 the plots obtained in this test and orientation are shown, where the raw data of the force-displacement

TABLE I Results of the sphere-doublet tests

| | Glue type | Peak force | Strength |
|---|---|---|---|
| Tensile | A | $100 \pm 32$ N | $12 \pm 4$ MPa |
| | E | $184 \pm 67$ N | $22 \pm 5$ MPa |
| Shear | A | $51 \pm 9$ N | $6.2 \pm 1.5$ MPa |
| | E | $82 \pm 26$ N | $10.1 \pm 1.6$ MPa |

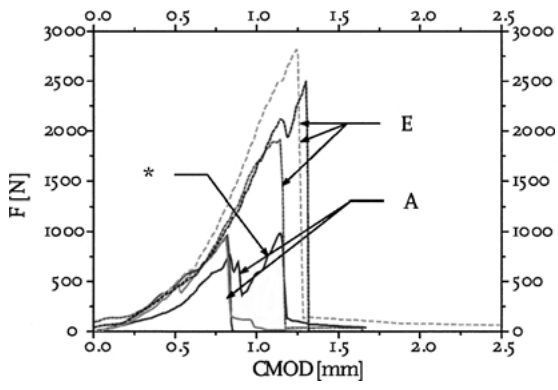


*Figure 4* Force-displacement plots of mode I fracture test on glue *A* and glue *E* model materials with (100) orientation. The asterisk (∗) labels the sample in which the crack plane shift was produced.

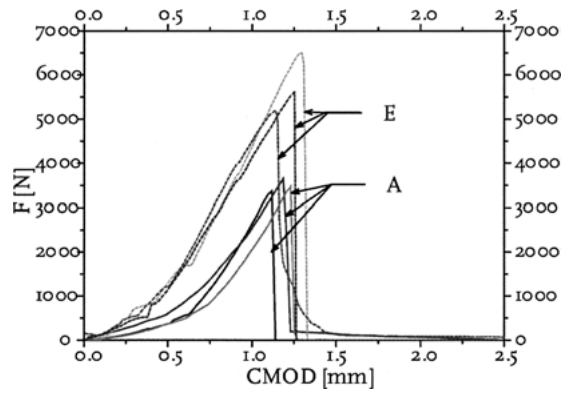


*Figure 5* Force-displacement plots of mode I fracture test on glue *A* and glue *E* model materials with (110) orientation.

of the testing head has been transformed into splitting force versus crack mouth opening displacement (CMOD). The CMOD is defined as the separation between the first glued spheres. The trigonometric relationship between CMOD and test head movement ($U$) is equal to:

$$\text{CMOD} = 2U \tan(\beta/2) \tag{6}$$

As it is seen in the graphic the average ultimate splitting force for glue $A$ is equal to $962 \pm 21$ N. For glue $E$ this force is equal to $2272 \pm 599$ N.

Because for the (110) orientation samples, producing a straight notch in the gluing step was not straightforward, and machining a notch was experimentally cumbersome, the procedure was slightly different: instead of introducing a wedge, a roller of 9.5 mm of diameter was placed in the middle of one of the side with [110] orientation. This roller transforms the vertical force of the head of the test machine into horizontal force that splits the material in two. Again, in Fig. 6 a sketch of the roller position with respect to the model material is presented. In this case, the initial crack length is equal to the gap between spheres, and equal to 2.07 mm. Once again, the raw data of the fracture test is transformed into a reaction force versus crack mouth opening displacement (CMOD). The applied force ($P$) is translated into the splitting force ($F$) with the same Equation 8, where $\beta$ now stands for the contact angle between the roller and the spheres assumed constant and equal to the initial contact angle, $\beta = 58.4°$.

The Force-CMOD graphs, as presented in Fig. 5, show that the ultimate fracture force is $3498 \pm 153$ N for glue $A$ and $5767 \pm 728$ N for glue $E$.

Photographs of the fractured samples for both orientations are shown in Fig. 7. The fracture path and failure behaviour (brittle) was similar in all samples for both glues. After fracture scanning electron microphotographs were taken of the fracture surfaces, shown in Fig. 8. In these pictures, it is clearly seen how the glue forms necks between the metal particles, joining the particles indeed. It is also seen how the glue is wiped out of the metal surface, leaving only small droplets, while remaining in the particle connection due to the surface tension. Closer attention also reveals that there is a lack of glue in the middle of the glue bond, in the exact point where the two metal spheres make contact. This glue gap has a size of $100 \pm 20$ $\mu$m, as shown in Fig. 9. This glue gap is due to the non-zero surface tension of the glue, and it is unavoidable when direct contact between metal particles is produced.

## 4. Finite element method simulation of stress patterns in particle couples

Finite element method analyses were used to model the tensile two-ball system to investigate where the fracture

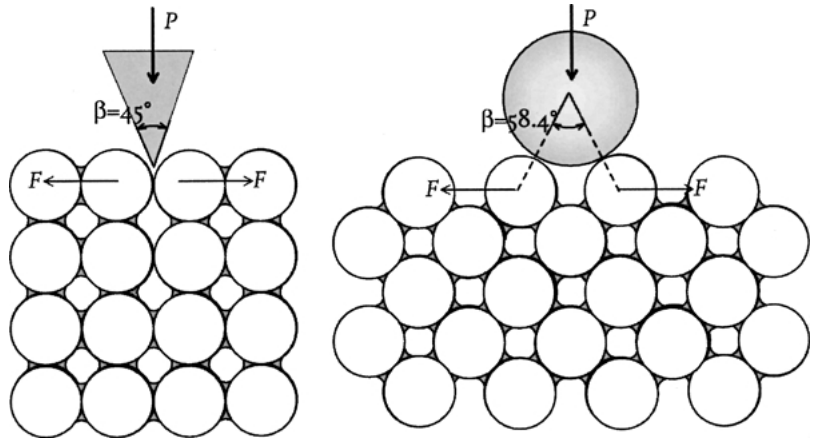


*Figure 6* Sketch of the wedges used for model material testing. At left the (100) orientation is presented, while at right the (110) orientation is shown.

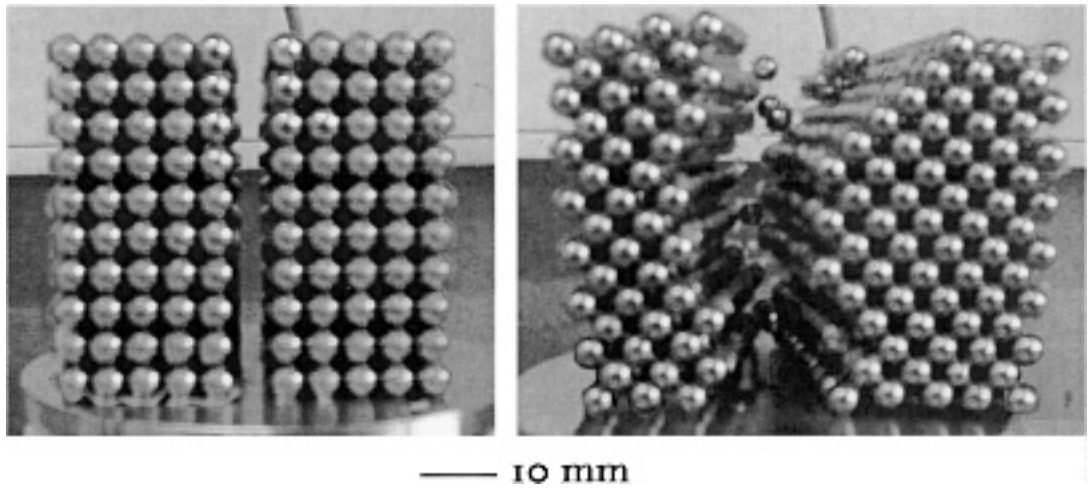


*Figure 7* Fracture of model materials (100)—left- and (110)—right-.

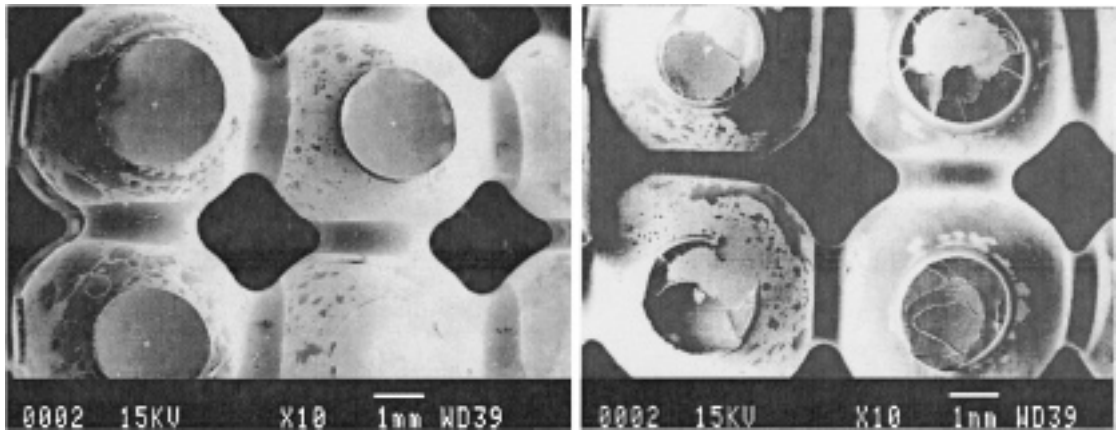


*Figure 8* Microphotograph of fracture between particles in glue *A* (left) and in glue *E* (right).

started and how the fracture behaviour changed as different parameters were varied. These are: material properties (particle and glue stiffness, plasticity of the glue) the glue neck geometrical parameters (diameter of the neck, curvature radius and diameter of the inner gap in the glue) and the applied force. The FRANC2DL [27, 28] package was used and several different ball diameters and different elastic modulus of glue were tried out, given all of them comparable results. The glue was modelled as linear elastic, which should hold true as a first approximation. A picture of the modelling of this system with a glue gap of 420 $\mu$m (largest modelled, but suitable for visualization proposes) and the $\sigma_{yy}$ stress distribution is shown in Fig. 10, where $y$ is the direction perpendicular to the contact plane. These analyses show that fracture is most probably initiated in the inner glue gap where stress concentration occurs. In that zone, due to the high stresses, plastic deformation of the glue is produced, forcing the fracture to start not in the middle of the glue neck, but in the interface glue-metal due to elastic mismatch of both materials, and switching later to the bulk glue in the case of glue *E*.

## 5. Discussion

Fracture in the neck of the glue is most probably initiated in the glue gap located in the middle of the glue neck, as it is seen in Fig. 9, due to this glue gap acting as an initial notch and stress concentrator. Finite element simulations also indicate that a stress concentration is present in the glue gap. Once the fracture starts in this glue gap, it propagates in a different way depending on the type of glue used.

When the fracture surfaces of the samples are examined, it is clearly seen how these surfaces differ depending on the glue used. Glue *A* presents a smooth surface with debonding in the glue-metal interface, while glue *E* shows secondary cracks and crack shift from one interface surface to another, indicating that glue *E* presents a better adhesion than glue *A*.

In the case of particle-pair test glue *A* surfaces are relatively smooth and the fracture runs along an interface between glue and metal particle, and therefore the crack is stable. When glue *E* samples are observed we see clearly how the fracture shifts from one interface to other, and various secondary cracks are formed.

It can also be appreciated how in the sphere doublet test, the values of shear strength are, approximately, one half of the values of the tensile strength for both glues (see Table II). This is in agreement with the Tresca's criterion, which states that:

$$\tau = \frac{1}{2}(\sigma_{\mathrm{I}} - \sigma_{\mathrm{III}}) \tag{7}$$

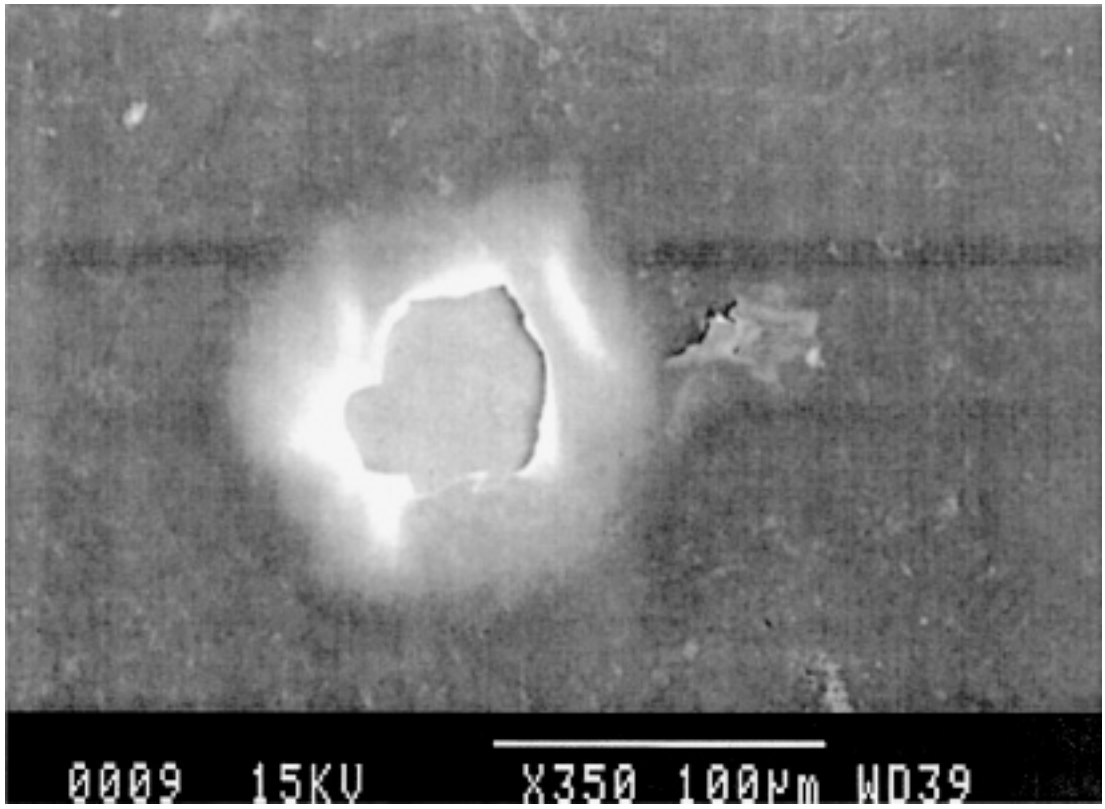


*Figure 9* Detail of the glue gap between two particles which acts as a fracture initiator.

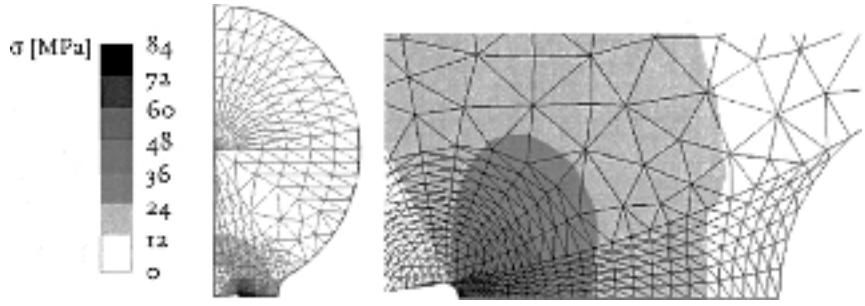


*Figure 10* Finite Element Methods results for a tensile test on 2 metal spheres joined together with glue and subjected to a plain stress test.

with $\sigma_I$ and $\sigma_{III}$ the first and third principal stresses and $\tau$ the shear strength. Because in our case:

$$\sigma_I \gg \sigma_{III} \tag{8}$$

we can approximate (7) as:

$$\tau = \frac{1}{2}\sigma_I \tag{9}$$

and therefore we can conclude that our model material behaves like a Tresca material.

The toughness of the complete model materials can be found with the maximum peak load using the formula [29] for wedge load opening samples. The stress intensity factor, $K_{Ic}$, is then related to the splitting force, $F$, via:

$$K_{Ic} = \frac{F}{b\sqrt{d}} Y(\alpha) \tag{10}$$

where $\alpha$ equals, again, to:

$$\alpha = \frac{a}{d} \tag{11}$$

and $b$ is the thickness of the sample, $d$ is the height of the sample, $a$ is the initial crack length and $Y(\alpha)$ is a

TABLE II Experimental data of the testing of the model materials

| Orientation | Glue | Fracture force | Toughness | FPZ size |
|---|---|---|---|---|
| (100) | A | $962 \pm 21$ N | $0.27 \pm 0.01$ MPa $m^{1/2}$ | $0.4 \pm 0.1$ mm |
| | E | $2272 \pm 580$ N | $0.70 \pm 0.18$ MPa $m^{1/2}$ | $1.0 \pm 0.5$ mm |
| (110) | A | $3498 \pm 180$ N | $0.58 \pm 0.03$ MPa $m^{1/2}$ | $8.8 \pm 2.5$ mm |
| | E | $5767 \pm 713$ N | $0.97 \pm 0.12$ MPa $m^{1/2}$ | $9.2 \pm 2.6$ mm |

correction factor [8], equal to:

$$Y(\alpha) = \frac{(1+\alpha)(0.8072 + 8.858\alpha - 30.23\alpha^2 + 41.088\alpha^3 - 24.15\alpha^4 + 4.951\alpha^5)}{(1-\alpha)^{1.5}} \quad (12)$$

Applying this formula we obtained the stress intensity values as shown in the Table II, both for the (100) orientation and for the (110) orientation.

With the values of toughness of the whole model material (Table II) and the values of maximum strength on particle-pairs, tensile for (100) and shear for (110) (Table I), the fracture process zone size is calculated with Equation 2. The obtained values are presented in Table II. These values show that the fracture process zone size in the (100) orientation is smaller than in the (110) orientation. That is, in case of the (100) orientation, for both glues, the fracture process zone only involves the first row of particles; only the particles in the crack tip are involved in the fracture. In case of the (110) orientation the fracture process zone involves typically two particles and the fracture is governed by a combination of the mechanical properties of particles surrounding the crack tip. This is seen if we analyse the relationship between model material peak force and particle pair strength.

The first thing to notice is that the ratio between the ultimate fracture forces of the two types of cubes (those glued with glue $A$, and those glued with glue $E$) is comparable to the ratio found between the fracture force of the single particle pair (glue $A$/glue $E$) and equal to $0.5 \pm 0.1$. It seems that there is a link between the particle-particle force and the overall macroscopic force, however complex, and there is little interaction between particles.

In the case of the (100) orientation, if we suppose that the bending moment is small and divide the ultimate fracture force by the depth of the sample, that is, by the number of particle pairs that are in front of the crack tip (ten particles) we obtain the ultimate tensile force per particle pair, $F'$. In glue $A$ this force equals $F' = 92.2 \pm 2.1$ N and in glue $E$ this force equals $227 \pm 60$ N. These values match the values we obtained for the tensile force between single particles ($100 \pm 32$ N for glue $A$ and $184 \pm 67$ N for glue $E$). This fact suggests that in this case, where the material behaves in a brittle way and the fracture propagates in a straight line, the ultimate fracture force is only dependent on the ultimate fracture force of the single particles in front of the crack tip. Once the applied force is high enough to overcome the ultimate fracture force of the single bond force, the fracture becomes dynamic and proceeds through the sample. This is in agreement with the fracture process zone being smaller than the particle size, as calculated before.

It is also seen in Fig. 4 that all the specimens except one (plot marked with an (∗)) broke in a similar brittle way along the plane containing the initial notch. In that particular sample, the crack path shifted from the plane of fracture to a neighbouring plane. This was due to the presence of a defect (consisting of a glue bridge between four particles) with higher strength at the crack tip. So the crack shifted to a neighbouring plane by breaking the neighbour bonds in shear mode, which has lower ultimate fracture force and then fracturing in that plane in the usual mode. This is an indication of how the existence of energy dissipative mechanisms influences the overall mechanical behaviour and produces a quasi-brittle fracture. It will be interesting, therefore, to proceed the research with this type of materials by introducing, controlling and modifying these types of defects, as it is expected that they could be made in such a way that they could resemble microcracking (by implementing weaker bonds) or bridging (by implementing defects strong enough to hold structural integrity after the crack tip). These types of materials are expected to be produced in the future, as they appear to be an interesting field of research.

If we do the same for the (110) samples we obtain an average force per particle pair in the crack tip equal to $175 \pm 8$ N for glue $A$ and $288 \pm 36$ N for glue $E$. This force is parallel to the cube face, so it has to be multiplied by $\sin(\pi/4)$ to obtain the components of shear and tensile force applied, leading to a shear and tensile force equal to $124 \pm 6$ N for glue $A$ and $204 \pm 25$ N for glue $E$. This force is clearly higher than the shear and the tensile fracture force, indicating that the fracture mechanism is not as simple as in the cube with (100) orientation. In this case, it appears that fracture does not depend on the maximum strength of the particle pair most near to the crack tip, but it is a more complex function of several particle pairs interacting in the neighbourhood. Again, this is in agreement with the fracture process zone size calculated before, in this case being larger than the particle size.

## 6. Conclusions

Model materials are a novel and useful tool in the study of quasi-brittle failure. They show a clear link between particle-particle mechanical behaviour and overall mechanical behaviour, that is, what will be the equivalent in a real material between mesostructure and macrostructure.

The fracture process zone is calculated and it seen how a different fracture process zone sizes result in a different number of particles involved in the fracture of the material. In case of (100) orientation, the small fracture process zone implied that only the particles close to the crack tip were involved in the fracture. In the case of the (110) orientation, the fracture was no longer dependent on the particles closest to the crack tip but it in a larger area around crack tip, in contrast with the (100) model materials.

It is also seen how, in case of (100) orientation, the existence of an energy dissipative mechanism (a glue bridge) resulted in a change in mechanical behaviour. This indicates that quasi-brittle behaviour is enhanced if energy-dissipative processes are introduced in the model material. Therefore, it is expected that further development in this field will produce further improvement of the results. This model material approach may be continued by further varying material parameters as

particle material (e.g. glass beads, hollow glass beads, polymer beads, . . .), particle shape or form factor, particle stacking (e.g., b.c.c., f.c.c., hexagonal compact, random.. . .), sample geometry or combination of different particle or bonding agent and controlling the type of defects.


## Acknowledgments

The authors wish to thank FOM-NWO for financial support.


## References


1. E. JIMÉNEZ-PIQUÉ, A. DORTMANS and G. DE WITH, to be published in *Mater. Sci. & Eng.* A.
2. C. Y. WANG, P. D. LIU and X. T. SUN, *Inter. J. Rock Mechan. and Mini. Sci. & Geomech. Abs.* **27**(1) (1990) 65.
3. K. DUAN, Y.-W. MAI and B. COTTERELL, *J. Euro. Cer. Soc.* **15** (1995) 1061.
4. P. REGNAUT and E. BRÜHWILER, *Eng. Frac. Mech.* **35**(1/2/3) (1990) 29.
5. J. J. DU, A. S. KOBAYASHI and N. M. HAWKINS, *ibid.* **35**(1) (1990) 15.
6. Z. K. GUO, A. S. KOBAYASHI and N. M. HAWKINS, *ibid.* **46**(6) (1993) 1041.
7. A. K. MAJI, C. OUYANG and S. P. SHAH, *J. Mater. Res.* **5**(1) (1990) 206.
8. H. MIHASHI, N. NOMURA and S. NIISEKI, *Cem. and Concr. Res.* **21** (1991) 737.
9. M. V. LYSAK, *Eng. Frac. Mech.* **55**(3) (1996) 443.
10. N. NOMURA, H. MIHASHI and M. IZUMI, *ibid.* **21** (1991) 545.
11. K. OTSUKA, "Fracture Toughness and Fracture Energy" (Balkema, 1989) p. 521.
12. K. OTSUKA and H. DATE, *Eng. Frac. Mech.* **65** (2000) 111.
13. A. HILLERBORG, M. MODÉER and P.-E. PETERSSON, *Cem. & Conc. Res.* **6** (1976) 773.
14. A. NEEDLEMAN, *J. Mech. Phys. Solids* **38**(3) (1990) 289.
15. V. TVERGAARD and J. W. HUTCHINSON, *ibid.* **40**(6) (1992) 1377.
16. B. N. COX and D. B. MARSHALL, *Acta Metall. Mater.* **42**(2) (1994) 341.
17. E. KRONER, *Int. J. Sol. Struct.* **3** (1968) 731.
18. Z. P. BAŽANT, T. B. BELYTSCHKO and T. P. CHANG, *J. Eng. Mech. Div. ASCE* **110**(12) (1984) 1666.
19. D. LASRY and T. BELYTSCHKO, *Int. J. Sol. Struct.* **24**(6) (1988) 581.
20. F. H. WITTMANN, "Frac. Mech. Conc. Struct.," in Proceedings of FraMCoS-1 (Masterdam, Elsevier, 1992) p. 391.
21. S. KAMIYA, T. YAMAUCHI and H. ABE, *Eng. Frac. Mech.* **66** (2000) 5173.
22. H. FESSLER and T. H. HYDE, *J. Strain. Anal.* **29**(3) (1993) 193.
23. K. J. VAN VLIET and S. SURESH, *Phil. Mag.* A **2002** (1993) 82.
24. D. BROEK, "Elementary Engineering Fracture Mechanics" (Kluwer Academic Publishers, Dordrecht, The Netherlands, 1986).
25. J. E. SRAWELY, *Int. J. Fract.* **12** (1976) 475.
26. W. F. BROWN and J. E. SRAWELY, ASTM STP 410 (1966) p. 12.
27. T. N. BITTENCOURT, PhD dissertation, Cornell University, USA, 1993.
28. P. WAWRZYNEK, FRANC2DL. Cornell University.
29. A. SAXENA and S. J. HUDAK, *Int. J. Fract.* **14**(5) (1978) 453.



*Received 6 November 2002*
*and accepted 26 June 2003*